AD-A064 702 HUGHES RESEARCH LABS MALIBU CALIF F/G 20/5
OPTICAL-MICROWAVE INTERACTIONS IN SEMICONDUCTOR DEVICES.(U)
JAN 79 H YEN, L FIGUEROA N00173-78-C-0192
UNCLASSIFIED NL

/ OF /
AD
AD 64702

END
DATE FILMED
4 -79
DDC

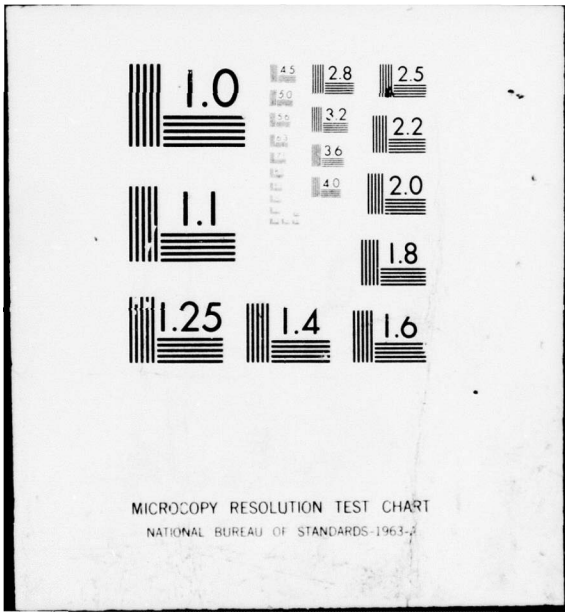
1.0
1.1
1.25
1.4
1.6
1.8
2.0
2.2
2.5
2.8
3.2
3.6
4.0
4.5
5.0
5.6
6.3
MICROCOPY RESOLUTION TEST CHART
NATIONAL BUREAU OF STANDARDS-1963-A

(12) LEVEL III

SC

A061224

AD A064702

OPTICAL–MICROWAVE INTERACTIONS IN SEMICONDUCTOR DEVICES

Huan-Wun Yen and Luis Figueroa

Hughes Research Laboratories

3011 Malibu Canyon Road

Malibu, CA 90265

January 1979

N00173–78–C–0192

Quarterly Report 2

For period 1 October 1978 through 31 December 1978

Approved for public release; distribution unlimited

DDC FILE COPY

Prepared For

NAVAL RESEARCH LABORATORY

4555 Overlook Avenue, S.W.

Washington, DC 20375

DDC

RECEIVED

FEB 16 1979

B

Sponsored by

ADVANCED RESEARCH PROJECTS AGENCY (DoD)

1400 Wilson Boulevard

Arlington, VA 22209

The views and conclusions contained in this document are those of the authors and should not be interpreted as necessarily representing the official policies, either expressed or implied, of the Defense Advanced Research Projects Agency or the U.S. Government.

79 02 12 013

UNCLASSIFIED

SECURITY CLASSIFICATION OF THIS PAGE (When Data Entered)

REPORT DOCUMENTATION PAGE	READ INSTRUCTIONS BEFORE COMPLETING FORM
1. REPORT NUMBER	2. GOVT ACCESSION NO. / 3. RECIPIENT'S CATALOG NUMBER
4. TITLE (and Subtitle) OPTICAL-MICROWAVE INTERACTIONS IN SEMICONDUCTOR DEVICES	5. TYPE OF REPORT & PERIOD COVERED Quarterly Report 2 1 Oct 1978-31 Dec 1978 / 6. PERFORMING ORG. REPORT NUMBER
7. AUTHOR(s) Huan-Wun Yen and Luis Figueroa	8. CONTRACT OR GRANT NUMBER(s) N00173-78-C-0192
9. PERFORMING ORGANIZATION NAME AND ADDRESS Hughes Research Laboratories 3011 Malibu Canyon Road Malibu, CA 90265	10. PROGRAM ELEMENT, PROJECT, TASK AREA & WORK UNIT NUMBERS
11. CONTROLLING OFFICE NAME AND ADDRESS Naval Research Laboratory 4555 Overlook Ave., S.W. Washington, D.C. 20375	12. REPORT DATE January 1979 / 13. NUMBER OF PAGES 55
14. MONITORING AGENCY NAME & ADDRESS(if different from Controlling Office)	15. SECURITY CLASS. (of this report) UNCLASSIFIED / 15a. DECLASSIFICATION DOWNGRADING SCHEDULE

16. DISTRIBUTION STATEMENT (of this Report)

Approved for public release; distribution unlimited.

17. DISTRIBUTION STATEMENT (of the abstract entered in Block 20, if different from Report)

18. SUPPLEMENTARY NOTES

19. KEY WORDS (Continue on reverse side if necessary and identify by block number)

Optical injection locking, Optical-microwave interactions, Si IMPATT oscillators, Mode locking of injection lasers, Millimeter-wave oscillators

20. ABSTRACT (Continue on reverse side if necessary and identify by block number)

The feasibility of achieving optical injection locking of millimeter-wave IMPATT oscillators was investigated by calculating the efficiency of subharmonic optical injection locking of IMPATT oscillators. Calculations were carried out by adding a time-varying reverse saturation current term, which was generated by the incident optical signal, to the IMPATT avalanche equation. The results indicated that a locking range on

→ next page

DD FORM 1 JAN 73 1473 EDITION OF 1 NOV 65 IS OBSOLETE

UNCLASSIFIED

SECURITY CLASSIFICATION OF THIS PAGE (When Data Entered)

79 02 12 013

the order of 100 MHz could be achieved for X-band IMPATT oscillators if modulated optical signal was converted into rf photocurrent efficiently.

The injection-locking characteristics of X-band Si IMPATT oscillators were further investigated by measuring the locking range as a function of locking gain. Subharmonic locking was used with a frequency ratio ranging from 3:1 to 8:1. It was observed that a locking range of several megahertz was achievable with an oscillator at 8.11 GHz. It was also noted that even subharmonic locking was preferred over odd subharmonic locking for our oscillators.

The transmission characteristics of two different Fabry-Perot resonators were studied in order to find an optimum external cavity configuration for injection lasers used in mode-locking experiments. The first resonator consisted of an injection laser of length ℓ_1 and a mirror located at a distance ℓ_o from the laser. The inner facet of the laser was coated with antireflection coating. The second resonator also consisted of an injection laser and a mirror except the laser facet was not coated. It was found that the second resonator had a higher Q factor and should be more suitable for mode-locking purposes.

TABLE OF CONTENTS

ACCESSION for
NTIS White Section
DDC Buff Section
UNANNOUNCED
JUSTIFICATION
BY
DISTRIBUTION/AVAILABILITY CODES
Dist. AVAIL. and/or SPECIAL
A

LIST OF ILLUSTRATIONS

PREFACE

The following personnel contributed to the research work reported here: H.W. Yen, L. Figueroa, M.K. Barnoski, A. Yariv (consultant), and D.F. Lewis.

SECTION 1

INTRODUCTION AND SUMMARY

The objectives of this program are to study the physics of microwave and millimeter-wave semiconductor devices under optical illumination, to study the techniques of modulating semiconductor lasers at microwave frequencies, and to combine the above two aspects to achieve optical control of microwave and millimeter-wave semiconductor devices. During the second quarter, we completed calculations on the feasibility of optical injection locking of millimeter-wave IMPATT oscillators, continued with the optical injection locking experiment of X-band Si IMPATT oscillators, and carried out calculations on the mode-locking characteristics of external-cavity GaAlAs injection lasers.

The feasibility of achieving optical injection locking of millimeter-wave IMPATT oscillators was investigated by calculating the efficiency of subharmonic optical injection locking of IMPATT oscillators. The calculations were carried out by adding a time-varying reverse saturation current term, which was generated by the incident optical signal, to the IMPATT avalanche equation. Solving the equation yielded a diode external current component related to the injected signal. This current was then taken as the injection source in the oscillator equivalent circuit to calculate the locking range. The results indicated that a locking range on the order of 100 MHz could be achieved for X-band IMPATT oscillators if modulated optical signal was converted into rf photocurrent efficiently.

The injection-locking characteristics of X-band Si IMPATT oscillators were further investigated by measuring the locking range as a function of locking gain. Subharmonic locking was used with a frequency ratio ranging from 3:1 to 8:1. A locking range of several megahertz was achievable with an oscillator at 8.11 GHz. Even subharmonic locking was preferable to odd subharmonic locking for our oscillators.

The transmission characteristics of two different Fabry-Perot resonators were studied to find an optimum external-cavity configuration for the injection-laser mode-locking experiment. The first resonator

consisted of an injection laser of length ℓ_1 and a mirror located at a distance ℓ_o from the laser. The inner facet of the laser was coated with an antireflection (AR) coating. Therefore, this combined resonator acted as a simple Fabry-Perot resonator with modes that are regularly spaced in frequency by $\Delta f = c/2(\ell_o + n\ell_1)$, where n is the index of refraction of the laser medium. The second resonator also consisted of an injection laser and a mirror; the laser facet, however, was not coated. In this case, we actually had three sets of Fabry-Perot resonators with lengths ℓ_o, $\ell_1 + \ell_o$, and ℓ_1. Therefore, the mode structure was more complicated, consisting of three sets of modes with frequency spacing $c/2\ell_o$, $c/2(\ell_o + n\ell_1)$, and $c/2n\ell_1$, respectively. However, since $\ell_o >> \ell_1$, the first two sets of modes would have roughly the same spacing and be located alongside one another. Since the second resonator was found to have a higher Q factor than the first, it might be easier to achieve mode-locking in this resonator.

SECTION 2

CALCULATIONS ON OPTICAL INJECTION LOCKING OF IMPATT OSCILLATORS

A. BASIC EQUATIONS

The equation that describes the avalanche current density J of an IMPATT diode is given by[1]

$$\frac{\tau_a}{2}\frac{dJ}{dt} = J\left[\int_0^{\ell_a} \alpha\, dx - 1\right] + J_s \quad , \tag{1}$$

where

$\tau_a = \ell_a/v$ is the avalanche zone transit time

ℓ_a is the avalanche zone length

α is the impact ionization coefficient

J_s is the reverse saturation current density

v is the saturated carrier velocity.

The ionization coefficient α is a function of the electric field in the avalanche region and can be approximated by the following expression:

$$\alpha = \alpha_o \left(\frac{E}{E_o}\right)^m \quad (m \approx 6 \text{ for silicon}) \quad .$$

Assume that the electric field distribution inside the IMPATT diode is as shown in Figure 1, where the field varies from its peak, E_p, down to the drift region value, E_d, with dE/dx constant. Therefore, it follows that

$$\int_0^{\ell_a} \alpha\, dx = \int_{E_p}^{E_d} \frac{\alpha}{\left(\frac{dE}{dx}\right)} dE = \left(\frac{E_p}{E_{po}}\right)^{m+1} - \left(\frac{E_d}{E_{po}}\right)^{m+1} \approx \left(\frac{E_p}{E_{po}}\right)^{m+1} \quad , \tag{2}$$

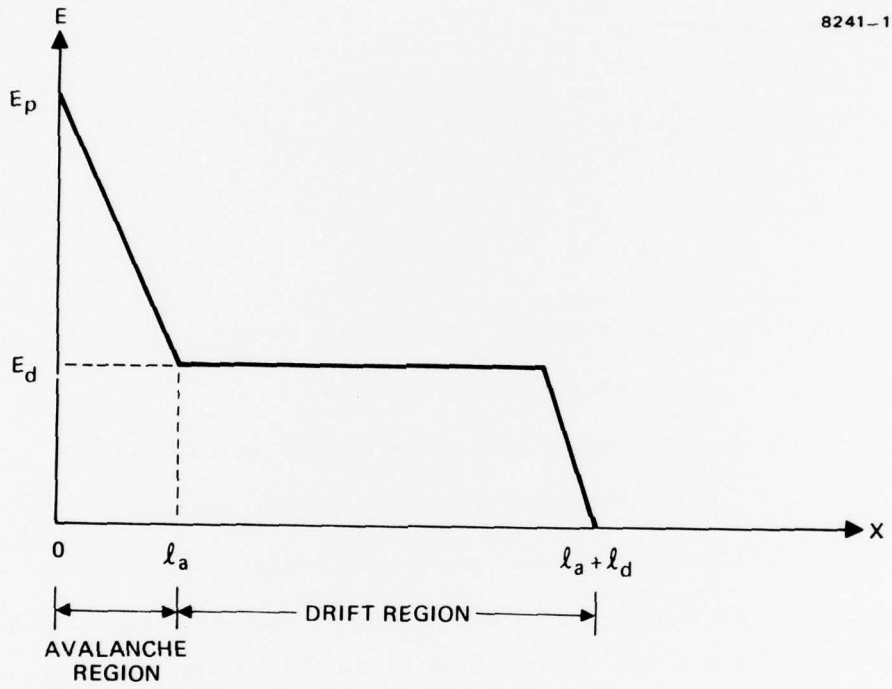

Figure 1. Electric field distribution inside an IMPATT diode.

where E_d^{m+1} has been neglected since $E_d^{m+1} << E_p^{m+1}$, and E_{po} is the peak field at breakdown under dc conditions (i.e., when $\int_0^{\ell_a} \alpha \, dx = 1$). Substituting Eq. 2 into Eq. 1 yields

$$\frac{\tau_a}{2} \frac{dJ}{dt} = J\left[\left(\frac{E_p}{E_{po}}\right)^{m+1} - 1\right] + J_s \quad . \tag{3}$$

The peak electric field E_p can be written as

$$E_p(t) = E_{po} - E_b + E_a \sin \omega t - \frac{1}{\varepsilon \tau_d} \int_{t-\tau_d}^{t} (\tau_d - t + t') \, J(t')dt' \quad , \tag{4}$$

where E_b is a constant, $E_a \sin \omega t$ is the field from the applied rf voltage, τ_d is the drift zone transit time, and $-1/\varepsilon\tau_d \int_{t-\tau_d}^{t} (\tau_d - t + t') \, J(t')dt'$ is a field resulting from the so-called space-charge effect. As an approximation, the effects of E_b and the space charge field can be treated by assuming that the carrier generation rate is sinusoidal but has a zero at $\pi - \delta$ instead of at π.[2] Therefore Eq. 4 becomes

$$E(t) = E_{po} + E_a \sin(\omega t + \delta) \quad ,$$

and Eq. 3 can be reduced to

$$\frac{dJ}{dt} = \frac{2(m+1)}{\tau_a} J \frac{E_a}{E_{po}} \sin(\omega t + \delta) + \frac{2}{\tau_a} J_s \quad , \tag{5}$$

where only the first term of the expansion of $(E_p/E_{po})^{m+1} - 1$ was kept.

B. FUNDAMENTAL OPTICAL INJECTION LOCKING

Suppose the IMPATT diode is illuminated by an optical signal modulated at frequency ω; then J_s can be written as

$$J_s = J_{so} + J_{s1} \sin(\omega t + \delta + \phi) \quad . \tag{6}$$

Substituting Eq. 6 into Eq. 5 yields

$$\frac{dJ}{dt} = J \frac{2(m+1)E_a}{\tau_a E_{po}} \sin(\omega t + \delta) + \frac{2}{\tau_a}\left[J_{so} + J_{s1} \sin(\omega t + \delta + \phi)\right] \tag{7}$$

Eq. 7 is of the form

$$\frac{dy}{dt} + P(t)\, y = Q(t) \quad , \tag{8}$$

whose solution is

$$y = e^{-\int P(t)dt} \int Q(t)\, e^{\int P(t)dt}\, dt + C\, e^{-\int P(t)dt} \quad , \tag{9}$$

where C is a constant.

Comparing Eqs. 7 and 8 gives

$$P(t) = -\frac{2(m+1)\,E_a}{\tau_a E_{po}} \sin(\omega t + \delta)$$

$$Q(t) = \frac{2}{\tau_a}\left[J_{so} + J_{s1} \sin(\omega t + \delta + \phi)\right]$$

and

$$\int P(t)dt = \frac{2(m+1)\,E_a}{\omega \tau_a E_{po}} \cos(\omega t + \delta) = x\cos(\omega t + \delta) \quad ,$$

where

$$x = \frac{2(m+1)}{\omega \tau_a} \frac{E_a}{E_{po}} \quad .$$

Therefore, the solution for J is given by

$$J = e^{-x\cos(\omega t+\delta)} \int \frac{2}{\tau_a} \left[J_{so} + J_{s1} \sin(\omega t + \delta + \phi) \right] e^{x\cos(\omega t+\delta)} dt$$

$$+ J_o e^{-x\cos(\omega t+\delta)} \quad . \tag{10}$$

With the help of the following relations

$$e^{x\cos(\omega t+\delta)} = I_o(x) + 2 \sum_{n=1}^{\infty} I_n(x) \cos n(\omega t + \delta)$$

$$e^{-x\cos(\omega t+\delta)} = I_o(x) + 2 \sum_{n=1}^{\infty} (-1)^n I_n(x) \cos n(\omega t + \delta) \quad ,$$

we can rewrite Eq. 10 as

$$J = J_o \left[I_o(x) + 2 \sum_{n=1}^{\infty} (-1)^n I_n(x) \cos n(\omega t+\delta) \right] + \frac{2}{\tau_a} \left[I_o(x) + 2 \sum_{n=1}^{\infty} (-1)^n I_n(x) \cos n(\omega t+\delta) \right]$$

$$\left\{ \left[J_{so} I_o(x) + J_{s1} I_1(x) \sin\phi \right] t - \frac{J_{s1} I_o(x)}{\omega} \cos(\omega t+\delta+\phi) \right.$$

$$+ \frac{2J_{so}}{\omega} \sum_{n=1}^{\infty} \frac{I_n(x)}{n} \sin n(\omega t+\delta) - \frac{J_{s1}}{\omega} \sum_{n=1}^{\infty} \frac{I_n(x)}{n+1} \cos\left[(n+1)(\omega t+\delta)+\phi \right]$$

$$\left. + \frac{J_{s1}}{\omega} \sum_{n=2}^{\infty} \frac{I_n(x)}{n-1} \cos\left[(n-1)(\omega t+\delta) - \phi \right] \right\} \quad . \tag{11}$$

By expanding the summations in Eq. 10 and keeping terms involving modified Bessel functions of order 0, 1, and 2 only, J becomes:

$$J = J_{dc} - 2\,J_{dc}\,\frac{I_1(x)}{I_o(x)}\cos(\omega t+\delta) + 2\,J_{dc}\,\frac{I_2(x)}{I_o(x)}\cos\,2(\omega t+\delta)$$

$$+\frac{2}{\tau_a}\,I_o(x)\left\{[J_{so}I_o(x) + J_{s1}\,I_1(x)\,\sin\phi]\,t - \frac{J_{s1}\,I_o(s)}{\omega}\cos(\omega t+\delta+\phi)\right.$$

$$+\frac{2\,J_{so}\,I_1(x)}{\omega}\sin(\omega t+\delta) + \frac{J_{so}\,I_2(x)}{\omega}\sin\,2(\omega t+\delta) - \frac{J_{s1}I_1(x)}{2\omega}\cos[2(\omega t+\delta)+\phi]$$

$$\left.-\frac{J_{s1}\,I_2(x)}{3\omega}\cos\,[3(\omega t+\delta)+\phi] + \frac{J_{s1}\,I_2(x)}{\omega}\cos(\omega t+\delta-\phi)\right\}$$

$$-\frac{4\,I_1(x)}{\tau_a}\left\{[J_{so}I_o(x)+J_{s1}I_1(x)\sin\phi]t\,\cos(\omega t+\delta)-\frac{J_{s1}I_o(x)}{2\omega}\{\cos[2(\omega t+\delta)+\phi]+\cos\phi\}\right.$$

$$+\frac{J_{so}I_1(x)}{\omega}\sin\,2(\omega t+\delta) + \frac{J_{so}I_2(x)}{2\omega}[\sin\,3(\omega t+\delta) + \sin(\omega t+\delta)]$$

$$-\frac{J_{s1}I_1(x)}{4\omega}[\cos\{3(\omega t+\delta)+\phi\}+\cos(\omega t+\delta+\phi)]-\frac{J_{s1}I_2(x)}{6\omega}[\cos\{4(\omega t+\delta)+\phi\}$$

$$\left.+\cos\,\{2(\omega t+\delta)+\phi\}] + \frac{J_{s1}I_2(x)}{2\omega}\,[\cos\{2(\omega t+\delta)-\phi\} + \cos\phi]\right\}$$

$$+\frac{4\,I_2(x)}{\tau_a}\left\{(J_{so}I_o(x)+J_{s1}I_1(x)\sin\phi)t\cos2(\omega t+\delta)-\frac{J_{s1}I_o(x)}{2\omega}[\cos\{3(\omega t+\delta)+\phi\}\right.$$

$$+\cos(\omega t+\delta-\phi)]+\frac{J_{so}I_1(x)}{\omega}[\sin3(\omega t+\delta)-\sin(\omega t+\delta)] + \frac{J_{so}I_2(x)}{2\omega}\sin4(\omega t+\delta)$$

$$-\frac{J_{s1}I_1(x)}{4\omega}[\cos\{4(\omega t+\delta)+\phi\}+\cos\phi]-\frac{J_{s1}I_2(x)}{6\omega}[\cos\{5(\omega t+\delta)+\phi\}+\cos(\omega t+\delta+\phi)]$$

$$\left.+\frac{J_{s1}I_2(x)}{2\omega}[\cos\{3(\omega t+\delta)+\phi\} + \cos(\omega t+\delta+\phi)]\right\}\quad , \qquad (12)$$

where $J_{dc} \equiv J_o\, I_o(x)$ is the dc current of the IMPATT diode. It is clear from Eq. 12 that, although the applied rf voltage across the IMPATT diode is sinusoidal, the corresponding rf current is not sinusoidal. However, we are interested in the fundamental component only. If we denote the fundamental component of J as $J_{(1)}$, then

$$J_{(1)} = -2\, J_{dc}\, \frac{I_1(x)}{I_o(x)} \cos(\omega t + \delta) + \frac{J_{so} I_1(x)\left[4\, I_o(x) - 6\, I_2(x)\right]}{\omega\tau_a} \sin(\omega t + \delta)$$

$$+ \frac{J_{s1}}{\omega\tau_a}\left[-2\, I_o^{\,2}(x) + I_1^{\,2}(x) + \frac{4}{3}\, I_2^{\,2}(x)\right] \cos(\omega t + \delta + \phi)$$

$$= -2\, J_{dc}\, \frac{I_1(x)}{I_o(x)} \left\{\cos(\omega t+\delta) - \frac{J_{so}}{J_{dc}}\, \frac{I_o(x)\left[2I_o(x)-3I_2(x)\right]}{\omega\tau_a} \sin(\omega t+\delta)\right\}$$

$$+ 2\, J_{s1} \left\{\frac{4I_2^{\,2}(x) - 6I_o^{\,2}(x) + 3I_1^{\,2}(x)}{6\,\omega\tau_a}\right\} \cos(\omega t + \delta + \phi) \quad . \quad (13)$$

Since $J_{so} << J_{dc}$, it follows that

$$\frac{J_{so}}{J_{dc}}\, \frac{I_o(x)[2I_o(x) - 3I_2(x)]}{\omega\tau_a} << 1 \quad .$$

We can rewrite $J_{(1)}$ as

$$J_{(1)} = -2\, J_{dc}\, \frac{I_1(x)}{I_o(x)} \cos(\omega t + \delta_s) + 2\, J_{s1}\, K(x) \cos(\omega t + \delta + \phi) \quad , \quad (14)$$

where

$$\delta_s \approx \sin^{-1} \frac{J_{so}}{J_{dc}}\, \frac{I_o(x)\,[2I_o(x) - 3I_2(x)]}{\omega\tau_a} + \delta$$

$$K(x) = \frac{4I_2^{\,2}(x) + 3I_1^{\,2}(x) - 6I_o^{\,2}(x)}{6\omega\tau_a} \quad .$$

The external circuit current, which is obtained by propagating $J_{(1)}$ through the drift region, is given by

$$J_{e(1)} = \frac{1}{\ell_d} \int_o^{\ell_d} J_{(1)}\, e^{-j\omega\frac{x}{v}}\, dx$$

$$= -\frac{2 \sin\left(\frac{\omega\tau_d}{2}\right)}{\left(\frac{\omega\tau_d}{2}\right)} \left\{ J_{dc}\, \frac{I_1(x)}{I_o(x)} \cos\left[\omega\left(t - \frac{\tau_d}{2}\right) + \delta_s\right] \right.$$

$$\left. - J_{s1}\, K(x) \cos\left[\omega\left(t - \frac{\tau_d}{2}\right) + \delta + \phi\right] \right\} \qquad (15)$$

To estimate the locking range, a lumped circuit is used,[3] as shown in Figure 2. Y_I, the admittance of the IMPATT diode, is equal to $G_1 + jB_1$, which can be found by dividing the first term in Eq. 15 by the rf voltage $V = -jV_1\, e^{j\omega t}$ and adding the depletion susceptance ωC_d:

$$Y_I = -j\, \frac{2 \sin \frac{\omega\tau_d}{2}}{\frac{\omega\tau_d}{2}}\, \frac{J_{dc} A\, I_1(x)}{V_1\, I_o(x)}\, e^{-j\left(\frac{\omega\tau_d}{2} - \delta_s\right)} + j\omega C_d \quad . \qquad (16)$$

The load admittance is

$$Y_L = (R + j\omega L)^{-1} = \frac{R}{R^2 + \omega^2 L^2} - j\, \frac{\omega L}{R^2 + \omega^2 L^2} \quad .$$

The injection current I_L is obtained by multiplying the second term in Eq. 15 by the area of the diode:

$$I_L = 2\, \frac{\sin \frac{\omega\tau_d}{2}}{\frac{\omega\tau_d}{2}}\, K(x)\, J_{s1}\, A\, e^{j\{\omega(t-\tau_d/2)+\delta+\phi\}} \quad , \qquad (17)$$

where A is the cross-sectional area of the diode.

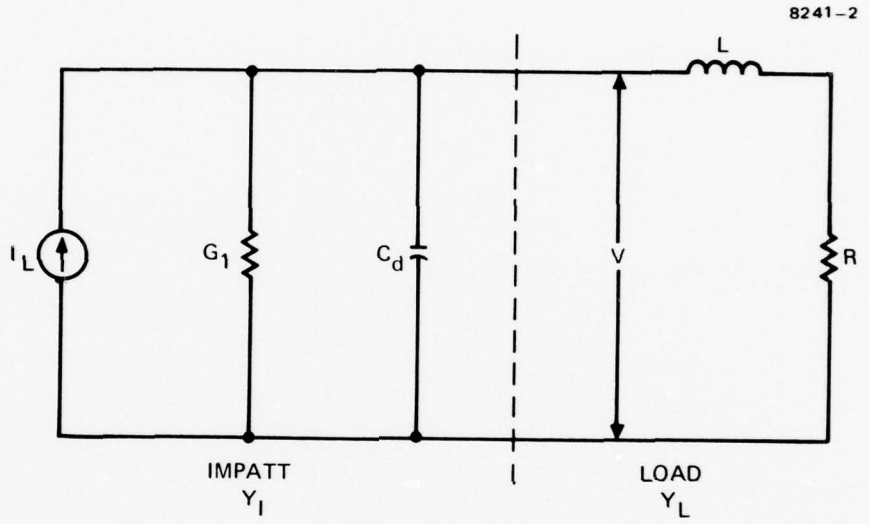

Figure 2. Equivalent circuit of an IMPATT oscillator used for injection locking calculations.

The circuit equation under locking is

$$I_L = (Y_I + Y_L)\, V \quad , \tag{18}$$

and the circuit equation under the free-running condition is

$$0 = \left[Y_I'(\omega_o) + Y_L(\omega_o)\right] V \quad . \tag{19}$$

In the following analysis, we will assume that

$$\frac{\omega\tau_d}{2} + \delta_s \approx \frac{\pi}{2} \quad , \quad \delta_s << \frac{\pi}{2} \quad .$$

In this case, Eq. 16 simplifies to

$$Y_I = -\frac{4}{\pi}\frac{I_1(x)\, I_{dc}}{I_o(x)\, V_1} + j\omega C_d = G_1 + j\, B_1 \quad . \tag{20}$$

The imaginary part of Eq. 19 gives

$$\omega_o C_d - \frac{\omega_o L}{R^2 + \omega_o^2 L^2} = 0 \text{ or } R^2 + \omega_o^2 L^2 = \frac{L}{C_d} \quad .$$

The imaginary part of Eq. 18 gives

$$\begin{aligned} I_m(I_L) &= \omega C_d - \frac{\omega L}{R^2 + \omega^2 L^2} \\ &= (\omega_o + \Delta\omega)\, C_d - \frac{(\omega_o + \Delta\omega)L}{R^2 + (\omega_o^2 + 2\Delta\omega\ \omega_o + \Delta\omega^2)L^2} \\ &\approx (\omega_o + \Delta\omega)\, C_d - \frac{(\omega_o + \Delta\omega)L}{R^2 + \omega_o^2 L^2}\left[1 - \frac{2\Delta\omega\ \omega_o L^2}{R^2 + \omega_o^2 L^2}\right] \\ &\approx 2\Delta\omega\ C_d\ (\omega_o^2\ C_d L) \approx 2\Delta\omega\ C_d \quad , \end{aligned} \tag{21}$$

where it is assumed that the series inductance resonates with the IMPATT capacitance at the operating frequency (i.e., $\omega_o^2 L\, C_d \approx 1$). From Eq. 17, it follows that $I_m(I_L)$ is given by

$$I_m(I_L) = -\frac{4}{\pi} K(x)\, I_{sl} \sin\phi \quad .$$

Therefore,

$$2\Lambda\omega = -\frac{4K(x)\, I_{sl}}{\pi\, V_1\, C_d} \sin\phi \quad . \tag{22}$$

The locking range is defined as the maximum $2\Lambda\omega$ achievable, and, from Eq. 22, $(2\Lambda\omega)_{max}$ is obtained by setting $\sin\phi = \pm 1$:

$$(2\Lambda\omega)_{max} = -\frac{4}{\pi} \frac{K(x)\, I_{sl}}{V_1\, C_d} \quad . \tag{23}$$

Since, from Eq. 20,

$$G_1 = -\frac{4}{\pi} \frac{I_1(x)}{I_o(x)} \frac{I_{dc}}{V_1} \quad ,$$

it follows that

$$(2\Delta\omega)_{max} = \left[-\frac{K(x)\, I_o(x)}{I_1(x)}\right] \frac{\omega I_{sl}}{Q I_{dc}} \quad , \tag{24}$$

where

$$Q = \left(\frac{\omega C_d}{G_1}\right)^{-1} = (\omega C_d R)^{-1} \quad .$$

Eq. 24 shows that the locking range is proportional to the optically generated current I_{sl} and is inversely proportional to the circuit Q and the bias dc current. We will use a few numerical examples to estimate $(2\Delta\omega)_{max}$.

One set of typical values is presented below:

$I_{dc} = 25$ mA $E_{po} = 2 \times 10^{7}$ V/m $I_{s1} = 20$ μA

$\ell_a = 1$ μm $v = 1 \times 10^{5}$ m/sec $Q = 20$

$\ell_d = 4$ μm $A = 10^{-8}$ m^2 $m = 6$

$\ell = \ell_a + \ell_d = 5$ μm $V_1 = 10$ V $f = 10$ GHz .

Based on these values, it follows that:

$\tau_a = \ell_a / v = 10^{-11}$ sec $\omega\tau_a = 0.63$

$$E_a = V_1/\ell = 2 \times 10^{6} \text{ V/m}$$

$$x = \frac{2(m+1)\, E_a}{\omega\tau_a\, E_{po}} = 2.22$$

$I_o(x) = 2.63$, $I_1(x) = 1.91$, $I_2(x) = 0.89$

$K(x) = -7.25$

$(2\Delta f)_{max} = 4.0$ MHz for $f = 10$ GHz.

If we take V_1 to be 15 V rather than 10 V, then

$x = 3.33$, $I_o(x) = 6.24$, $I_1(x) = 5.23$, $I_2(x) = 2.97$,

$K(x) = -30.76$

and

$(2\Delta f)_{max} = 14.7$ MHz for $f = 10$ GHz.

C. FIRST SUBHARMONIC OPTICAL INJECTION LOCKING ($\omega_{IMPATT}:\omega_{injection} = 2:1$)

Assume that the optically generated current is at the first subharmonic and that the reverse saturation current is given by

$$J_s = J_{so} + J_{s1/2} \sin \frac{1}{2} (\omega t + \delta + \phi) \quad . \tag{25}$$

Again we use Eq. 5 to solve for the avalanche current J:

$$J = J_o \left\{ I_o(x) + 2 \sum_{n=1}^{\infty} (-1)^n I_n(x) \cos n(\omega t + \delta) \right\} + \frac{2}{\tau_a} \left\{ I_o(x) \right.$$

$$\left. + 2 \sum_{n=1}^{\infty} (-1)^n I_n(x) \cos n(\omega t + \delta) \right\} \left\{ J_{so} I_o(x) t \right.$$

$$- \frac{2 J_{s1/2} \; I_o(x)}{\omega} \cos \frac{1}{2} (\omega t + \delta + \phi)$$

$$+ \frac{2 J_{so}}{\omega} \sum_{n=1}^{\infty} \frac{I_n(x)}{n} \sin n(\omega t + \delta) - \frac{2 J_{s1/2}}{\omega} \sum_{n=1}^{\infty} \frac{I_n(x)}{2n+1} \cos \left[\left(n + \frac{1}{2} \right) (\omega t + \delta) + \frac{\phi}{2} \right]$$

$$\left. + \frac{2 J_{s1/2}}{\omega} \sum_{n=1}^{\infty} \frac{I_n(x)}{2n-1} \cos \left[\left(n - \frac{1}{2} \right) (\omega t + \delta) - \frac{\phi}{2} \right] \right\} \quad .$$

Expanding the summations up to n = 2 and collecting terms involving cos ωt, sin ωt, cos 1/2 ωt, and sin 1/2 ωt yields

$$J = -2\, J_{dc}\, \frac{I_1(x)}{I_o(x)} \cos\,(\omega t + \delta_s) + \frac{4\, J_{s1/2}}{\omega \tau_a} \left\{\left(\left[\frac{2}{15}\, I_2^2(x) - \frac{2}{3}\, I_1^2(x) - I_o^2(x)\right]\right.\right.$$

$$\left. + 2\, I_1(x)\left[I_o(x) - \frac{1}{3}\, I_2(x)\right] \cos\phi\right) \cos\,\frac{1}{2}\,(\omega t + \delta + \phi)$$

$$\left. + 2\, \sin\phi\; I_1(x)\left[I_o(x) - \frac{1}{3}\, I_2(x)\right] \sin\,\frac{1}{2}\,(\omega t + \delta + \phi)\right\}$$

$$= -2\, J_{dc}\, \frac{I_1(x)}{I_o(x)} \cos\,(\omega t + \delta_s) + J_{1/2} \quad ,$$

where

$$J_{1/2} = A_1 \cos\,\frac{1}{2}\,(\omega t + \delta + \phi) + A_2 \sin\,\frac{1}{2}\,(\omega t + \delta + \phi)$$

$$A_1 = \frac{4\, J_{s1/2}}{\omega \tau_a} \left\{\frac{2}{15}\, I_2^2(x) - \frac{2}{3}\, I_1^2(x) - I_o^2(x) + 2\, \cos\phi\; I_1(x)\left[I_o(x) - \frac{1}{3}\, I_2(x)\right]\right\}$$

$$A_2 = \frac{4\, J_{s1/2}}{\omega \tau_a} \left\{2\, \sin\phi\; I_1(x)\, \left[I_o(x) - \frac{1}{3}\, I_2(x)\right]\right\}$$

and, therefore,

$$J_{1/2} = \left[A_1^2 + A_2^2\right]^{1/2} \left\{\frac{A_1}{\sqrt{A_1^2 + A_2^2}} \cos\,\frac{1}{2}\,(\omega t + \delta + \phi) + \frac{A_2}{\sqrt{A_1^2 + A_2^2}} \sin\frac{1}{2}\,(\omega t + \delta + \phi)\right\}$$

$$= \left[A_1^2 + A_2^2\right]^{1/2} \sin\,\frac{1}{2}\,(\omega t + \delta + \phi + \theta)$$

$$= J_{1/2o} \sin\,\frac{1}{2}\,(\omega t + \delta + \phi_s) \quad , \qquad (26)$$

where

$$\phi_s = \phi + \theta \text{ , and } \tan\,\frac{\theta}{2} = \frac{A_1}{A_2} \quad .$$

It is clear that θ is a function of ϕ. A plot of θ versus ϕ is shown in Figure 3.

The avalanche current component at 1/2 ωt (i.e., $J_{1/2}$) can modify the rf electric field in the avalanche region through the space-charge effect. The modified electric field is E + ΔE with ΔE given by:

$$\Delta E(t) = -\frac{1}{\varepsilon \tau_d} \int_{t-\tau_d}^{t} (\tau_d - t + t')\, J_{1/2}(t')\, dt' \quad .$$

Since $J_{1/2}(t')$ varies with a period of $4\pi/\omega$, it can be approximated as a constant during the integration time interval:

$$\Delta E(t) \approx -\frac{\tau_d}{2\varepsilon} J_{1/2}(t)$$

$$\approx -\frac{\tau_d}{2\varepsilon} J_{1/2o} \sin \frac{1}{2}(\omega t + \delta + \phi_s)$$

$$\equiv -E_b \sin \frac{1}{2}(\omega t + \delta + \phi_s) \quad , \qquad (26)$$

where

$$E_b = \frac{\tau_d J_{1/2o}}{2\varepsilon} \quad .$$

We can now solve for the avalanche current using the equation

$$\frac{dJ}{dt} = \frac{2J\,(m+1)}{\tau_a}\left[\frac{E_a}{E_{po}} \sin(\omega t + \phi) - \frac{E_b}{E_{po}} \sin \frac{1}{2}(\omega t + \delta + \phi_s)\right] ,$$

whose solution is

$$J = J_o\, e^{-x\cos(\omega t+\delta)+y\cos\frac{1}{2}(\omega t+\delta+\phi)} \quad , \qquad (27)$$

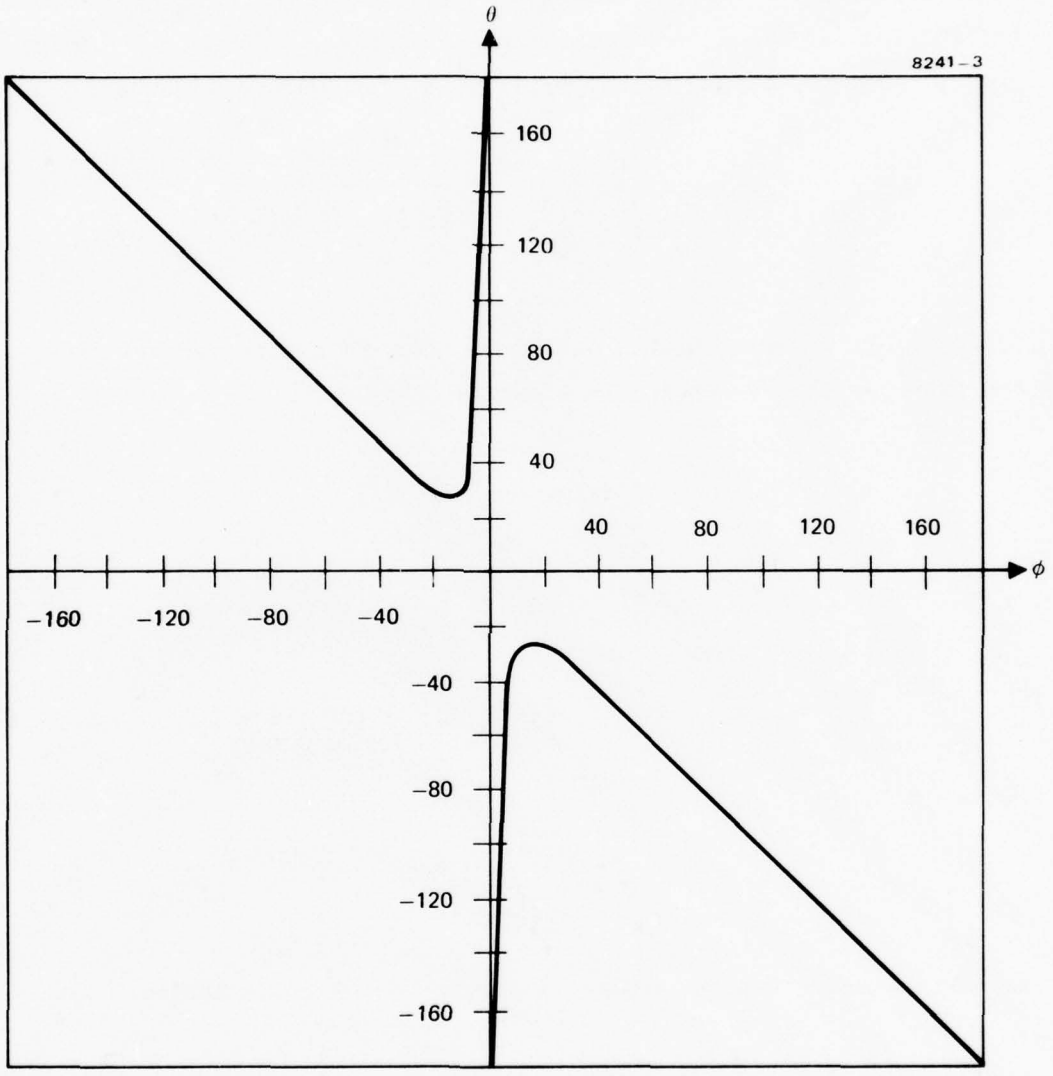

Figure 3. Plot of angle θ versus angle ϕ.

where

$$x = \frac{2\ (m+1)\ E_a}{\omega\tau_a\ E_{po}}\ ,\quad y = \frac{4\ (m+1)\ E_b}{\omega\tau_a\ E_{po}}\ .$$

From Eq. 27,

$$\begin{aligned}
J = J_o \Big\{ & I_o(x) - 2I_1(x)\cos(\omega t + \delta) + 2I_2(x)\cos 2\ (\omega t + \delta) \\
& - 2I_3(x)\cos 3\ (\omega t + \delta) + \cdots \Big\} \\
& \Big\{ I_o(y) + 2I_1(y)\cos\tfrac{1}{2}\ (\omega t + \delta + \phi_s) + 2I_2(y)\cos\ (\omega t + \delta + \phi_s) \\
& + 2I_3(y)\cos\tfrac{3}{2}\cos\ (\omega t + \delta + \phi_s) \\
& + 2I_4(y)\cos 2\ (\omega t + \delta + \phi_s) + \cdots \Big\} \\
= J_o \Big\{ & I_o(x)\ I_o(y) - 2I_1(x)\ I_o(y)\cos\ (\omega t + \delta) \\
& + 2I_o(x)\ I_1(y)\cos\tfrac{1}{2}\ (\omega t + \delta + \phi_s) + 2I_o(x)\ I_2(y)\cos\ (\omega t + \delta + \phi_s) \\
& + 4I_2(x)\ I_2(y)\cos 2\ (\omega t + \delta)\cos\ (\omega t + \delta + \phi_s) + \cdots \Big\}\ .
\end{aligned}$$

By retaining terms involving ωt only,

$$
\begin{aligned}
J &= J_o \Big\{ I_o(x)\, I_o(y) - 2 I_1(x)\, I_o(y) \cos(\omega t + \delta) \\
&\quad + 2 I_o(x)\, I_2(y) \cos(\omega t + \delta + \phi_s) \\
&\quad + 2 I_2(x)\, I_2(y) \cos(\omega t + \delta - \phi_s) + \cdots \Big\} \\
&= J_o\, I_o(x)\, I_o(y) \left\{ 1 - 2 \frac{I_1(x)}{I_o(x)} \cos(\omega t + \delta) + 2 \frac{I_2(y)}{I_o(y)} \cos(\omega t + \delta + \phi_s) \right. \\
&\quad \left. + 2 \frac{I_2(x)\, I_2(y)}{I_o(x)\, I_o(y)} \cos(\omega t + \delta - \phi_s) + \cdots \right\} \\
&= J_{dc} - 2 J_{dc} \frac{I_1(x)}{I_o(x)} \cos(\omega t + \delta) + 2 J_{dc} \frac{I_2(y)}{I_o(y)} \left\{ \cos(\omega t + \delta + \phi_s) \right. \\
&\quad \left. + \frac{I_2(x)}{I_o(x)} \cos(\omega t + \delta - \phi_s) \right\} \\
&= J_{dc} - 2 J_{dc} \frac{I_1(x)}{I_o(x)} \cos(\omega t + \delta) + 2 J_{dc} \frac{I_2(y)}{I_o(y)} \left[1 + 2 \frac{I_2(x)}{I_o(x)} \cos 2\phi_s \right. \\
&\quad \left. + \frac{I_2^2(x)}{I_o^2(x)} \right]^{1/2} \cos(\omega t + \delta + \phi_s - \psi) \quad ,
\end{aligned}
$$

where

$$
\tan \psi = \frac{\dfrac{I_2(x)}{I_o(x)} \sin 2\phi_s}{1 + \dfrac{I_2(x)}{I_o(x)} \cos 2\phi_s} \quad .
$$

The external circuit current is then given by

$$J_e = J_{dc} - \frac{2 \sin \frac{\omega\tau_d}{2}}{\frac{\omega\tau_d}{2}} \left\{ J_{dc} \frac{I_1(x)}{I_o(x)} \cos \left[\omega \left(t - \frac{\tau_d}{2} \right) + \delta \right] \right.$$

$$- J_{dc} \frac{I_2(y)}{I_o(y)} \left[1 + 2 \frac{I_2(x)}{I_o(x)} \cos 2\phi_s \right.$$

$$\left. \left. + \frac{I_2^2(x)}{I_o^2(x)} \right]^{1/2} \cos \left[\omega \left(t - \frac{\tau_d}{2} \right) + \delta + \phi_s - \psi \right] \right\} \quad . \tag{28}$$

The injection current is given by

$$I_L = 2 I_{dc} \frac{\sin \frac{\omega\tau_d}{2}}{\frac{\omega\tau_d}{2}} \frac{I_2(y)}{I_o(y)} \left[1 + 2 \frac{I_2(x)}{I_o(x)} \cos 2\phi_s \right.$$

$$\left. + \frac{I_2^2(x)}{I_o^2(x)} \right]^{1/2} \cos \left[\omega \left(t - \frac{\tau_d}{2} \right) + \delta + \phi_s - \psi \right] \quad .$$

If we assume that $\frac{\omega\tau_d}{2} + \delta \approx \frac{\pi}{2}$ and $\delta << \frac{\pi}{2}$, then, from Eq. 18, we can write:

$$2 \Delta\omega = \frac{I_{dc}}{C_d V_1} \frac{4}{\pi} \frac{I_2(y)}{I_o(y)} \left[1 + 2 \frac{I_2(x)}{I_o(x)} \cos 2\phi_s + \frac{I_2^2(x)}{I_o^2(x)} \right]^{1/2} \sin (\phi_s - \psi)$$

or

$$2 \Delta\omega = \left[\frac{I_o(x)\ I_2(y)}{I_1(x)\ I_o(y)} \right] \frac{\omega}{Q} \left\{ 1 + 2 \frac{I_2(x)}{I_o(x)} \cos 2\phi_s + \frac{I_2^2(x)}{I_o^2(x)} \right\}^{1/2} \sin (\phi_s - \psi) \quad . \tag{29}$$

Therefore, the locking range is the maximum value of the right side of Eq. 29. We will calculate the magnitude of $2\Delta\omega$ for a number of ϕ angles. The following numerical parameters are used:

$$I_{s1/2} = 20\ \mu A\ , \qquad I_{dc} = 25\ mA\ , \qquad V_1 = 15\ V\ .$$

$$Q = 20\ , \qquad \ell_a = 1\ \mu m\ , \qquad \ell_d = 4\ \mu m\ .$$

$$\varepsilon = 11\ \varepsilon_o\ , \qquad E_{po} = 2 \times 10^7\ V/m\ , \qquad A = 10^{-8}\ m^2$$

$$v = 10^5\ m/sec\ , \qquad f = 10\ GHz$$

$$x = 3.33\ , \quad I_o(x) = 6.24\ , \quad I_1(x) = 5.23\ , \quad I_2(x) = 2.97$$

$$A_1 = -7.11 \times 10^5 + 6.97 \times 10^5 \cos\phi$$

$$A_2 = 6.97 \times 10^5 \sin\phi\ .$$

For

$$\phi = 0°, \quad \theta = 180°, \quad \phi_s = -180°, \text{ and } \psi = 0°\ ,$$

we have

$$\sin(\phi_s - \psi) = 0 \quad \text{and} \quad 2\Delta\omega = 0\ .$$

For

$$\phi = 10°\ , \ \theta = -22.97°\ , \quad \phi_s = -12.97°\ , \quad \psi = -8.29°$$

$$y = 0.06, \text{ and } \sin(\phi_s - \psi) = -8.16 \times 10^{-2}\ ,$$

we have

$$2\Delta f = 0.03\ MHz.$$

For

$$\phi = 30^\circ , \quad \theta = -34.3^\circ , \quad \phi_s = -4.3^\circ , \quad \psi = -2.2^\circ$$

$$y = 0.166, \text{ and } \quad \sin (\phi_s - \psi) = -0.04 ,$$

we have

$$2\Delta f = 0.12 \text{ MHz}.$$

For

$$\phi = 60^\circ , \quad \theta = -61.97^\circ , \quad \phi_s = -1.97^\circ , \quad \psi = -1.27^\circ$$

$$y = 0.32 , \text{ and } \quad \sin (\phi_s - \psi) = 1.27 \times 10^{-2} ,$$

we have

$$2\Delta f = 0.124 \text{ MHz}.$$

For

$$\phi = 90^\circ , \quad \theta = -91.14^\circ , \quad \phi_s = -1.14^\circ , \quad \psi = -0.74^\circ$$

$$y = 0.45 , \text{ and } \quad \sin (\phi_s - \psi) = 6.98 \times 10^{-3} ,$$

we have

$$2\Delta f = 0.12 \text{ MHz}.$$

From the above numerical values, we conclude that the first subharmonic optical injection locking is relatively inefficient.

D. SECOND SUBHARMONIC OPTICAL INJECTION LOCKING ($\omega_{IMPATT}:\omega_{injection} = 3:1$)

If we let $J_s = J_{so} + J_{s1/3} \sin 1/3 (\omega t + \delta + \phi)$ and solve for J in Eq. 5, then

$$J = J_o \left\{ I_o(x) + 2 \sum_{n=1}^{\infty} (-1)^n I_n(x) \cos n(\omega t + \delta) \right\} + \frac{2}{\tau_a} \left\{ I_o(x) \right.$$

$$\left. + 2 \sum_{n=1}^{\infty} (-1)^n I_n(x) \cos n(\omega t + \delta) \right\}$$

$$\left\{ J_{so} I_o(x) t - \frac{3 J_{s1/3} I_o(x)}{\omega} \cos \frac{1}{3} (\omega t + \delta + \phi) \right.$$

$$+ \frac{2 J_{so}}{\omega} \sum_{n=1}^{\infty} \frac{I_n(x)}{n} \sin n (\omega t + \delta)$$

$$- \frac{3 J_{s1/3}}{\omega} \sum_{n=1}^{\infty} \frac{I_n(x)}{3n+1} \cos \left[\left(n + \frac{1}{3} \right) \left(\omega t + \delta \right) + \frac{\phi}{3} \right]$$

$$\left. + \frac{3 J_{s1/3}}{\omega} \sum_{n=1}^{\infty} \frac{I_n(x)}{3n-1} \cos \left[\left(n - \frac{1}{3} \right) \left(\omega t + \delta \right) - \frac{\phi}{3} \right] \right\} \quad .$$

Terms involving cos 1/3 $(\omega t + \delta + \phi)$ are grouped to give

$$J_{1/3} = \frac{J_{s1/3}}{\omega \tau_a} \left[\frac{12}{35} I_2^2(x) - \frac{3}{2} I_1^2(x) - 6 I_o^2(x) \right] \cos \frac{1}{3} (\omega t + \delta + \phi)$$

$$= J_{1/3o} \cos \frac{1}{3} (\omega t + \delta + \phi) \quad .$$

The electric field is modified by ΔE, which is given by

$$\Delta E = \frac{J_{1/3o} \tau_d}{2\varepsilon} \equiv E_{b1/3} \quad .$$

Therefore, the new rf field is

$$E = E_a \sin(\omega t + \delta) - E_b \cos\frac{1}{3}(\omega t + \delta + \phi) \quad ,$$

and the new avalanche current is

$$J = J_o \left[e^{-x\cos(\omega t+\delta)}\right]\left[e^{-y\sin\frac{1}{3}(\omega t+\delta+\phi)}\right] \quad ,$$

where

$$x = \frac{2(m+1)E_a}{\omega\tau_a E_{po}} \quad , \quad y = \frac{6(m+1)E_{b1/3}}{\omega\tau_a E_{po}} \quad .$$

Thus,

$$J = J_o \left\{I_o(x) - 2I_1(x)\cos(\omega t + \delta) + 2I_2(x)\cos 2(\omega t + \delta) + \cdots\right\}$$

$$\left\{I_o(y) + 2I_1(y)\sin\frac{1}{3}(\omega t + \delta + \phi) - 2I_2(y)\cos\frac{2}{3}(\omega t + \delta + \phi)\right.$$

$$\left. - 2I_3(y)\sin(\omega t + \delta + \phi) + \cdots\right\}$$

$$= J_o \left\{I_o(x)\, I_o(y) - 2I_o(y)\, I_1(x)\cos(\omega t + \delta) + 2I_o(y)\, I_2(x)\cos 2(\omega t + \delta)\right.$$

$$+ 2I_o(x)\, I_1(y)\sin\frac{1}{3}(\omega t + \delta + \phi) - 2I_o(x)\, I_2(y)\cos\frac{2}{3}(\omega t + \delta + \phi)$$

$$- 2I_o(x)\, I_3(y)\sin(\omega t + \delta + \phi)$$

$$\left. -4I_2(x)\, I_3(y)\cos 2(\omega t + \delta)\sin(\omega t + \delta + \phi) + \cdots\right\} \quad .$$

If we keep only terms involving ωt, then

$$J = J_o \Big\{ I_o(x)\, I_o(y) - 2I_o(y)\, I_1(x) \cos(\omega t + \delta)$$

$$- 2I_o(x)\, I_3(y) \sin(\omega t + \delta + \phi)$$

$$+ 2I_2(x)\, I_3(y) \sin(\omega t + \delta - \phi) + \cdots \Big\}$$

$$= J_{dc} - 2J_{dc} \frac{I_1(x)}{I_o(x)} \cos(\omega t + \delta) - 2J_{dc} \frac{I_3(y)}{I_o(y)} \left[1 - 2 \frac{I_2(x)}{I_o(x)} \cos 2\phi + \left(\frac{I_2(x)}{I_o(x)} \right)^2 \right]^{1/2} \cos(\omega t + \delta + \phi - \psi) \quad ,$$

where

$$\tan \psi = \frac{1 - \dfrac{I_2(x)}{I_o(x)} \cos 2\phi}{\dfrac{I_2(x)}{I_o(x)} \sin 2\phi} \quad .$$

Therefore, the injection current is

$$J_L = J_{1/3^A} = -2I_{dc} \frac{I_3(y)}{I_o(y)} \frac{\sin \dfrac{\omega\tau_d}{2}}{\dfrac{\omega\tau_d}{2}} \left\{ 1 - 2 \frac{I_2(x)}{I_o(x)} \cos 2\phi + \left(\frac{I_2(x)}{I_o(x)} \right)^2 \right\}^{1/2}$$

$$\cos \left\{ \omega \left(t - \frac{\tau_d}{2} \right) + \delta + \phi - \psi \right\} \quad ,$$

and the locking range is

$$2\Delta\omega = \left[\frac{I_o(x)\, I_3(y)}{I_1(x)\, I_o(y)} \right] \frac{\omega}{Q} \left[1 - 2 \frac{I_2(x)}{I_o(x)} \cos 2\phi + \frac{I_2^2(x)}{I_o^2(x)} \right]^{1/2} \sin(\phi - \psi) \quad .$$

Use the following numerical values:

$$I_{s1/3} = 20\ \mu A\ , \qquad I_{dc} = 25\ mA\ , \qquad V_1 = 15\ V$$

$$Q = 20\ , \qquad \ell_a = 1\ \mu m, \qquad \ell_d = 4\ \mu m$$

$$\varepsilon = 11\varepsilon_o\ , \qquad E_{po} = 2 \times 10^7\ V/m\ , \qquad A = 10^{-8}\ m^2$$

$$v = 10^5\ m/sec\ , \qquad f = 10\ GHz\ .$$

From these, we get

$$x = 3.33\ , \qquad I_o(x) = 6.24\ , \qquad I_1(x) = 5.23\ , \qquad I_2(x) = 2.97$$

$$J_{1/3o} = -8.62 \times 10^{-5}, \quad y = 0.6\ , \qquad \frac{I_3(y)}{I_o(y)} = 4.21 \times 10^{-3}\ .$$

For

$\phi = 0°$ and $\psi = 90°$, we have $2\Delta f = 1.32$ MHz.

For

$\phi = 15°$ and $\psi = 68°$, we have $2\Delta f = 1.27$ MHz.

For

$\phi = 30°$ and $\psi = 61.6°$, we have $2\Delta f = 0.99$ MHz.

For

$\phi = 60°$ and $\psi = 71.6°$, we have $2\Delta f = 0.66$ MHz.

E. DISCUSSION

It is clear from the above calculations that, to increase the locking range, both x and y should be made as large as possible, where

$$x = \frac{2\,(m+1)\,E_a}{\omega\tau_a\,E_{po}}$$

$$y = \frac{2\,(m+1)\,n\,J_{1/n}\,\sigma\,\tau_d}{\omega\tau_a\,E_{po}\,2\varepsilon} \quad ,$$

$$E_a = V_1/\ell \quad .$$

E_a is the rf electric field in the diode. Therefore, in a short diode, E_a is larger for a given V_1. On the other hand, the optimum oscillation frequency of a shorter diode is higher. Thus, the optimal situation seems to be to operate the diode in the lower portion of its frequency band. Our limited experimental results seem to indicate that this is the case. The best way to increase y is to have large optically generated current. Numerical values used in the previous calculations do not represent the best situation. A simple calculation reveals that 1 mW of optical power at rf frequency can generate up to 660 μA of rf photocurrent under ideal conditions. This would mean a locking range of 250 MHz for the case of $\omega_{osc} : \omega_{injection} = 3:1$. Therefore, it is important to investigate means of generating efficient, high-frequency, modulated optical sources.

Preliminary experiments on subharmonic optical injection locking of X-band Si IMPATT oscillators have shown a locking range of close to 7 MHz with a 4 to 1 frequency ratio. The photocurrent (rf) amplitude in these experiments is estimated to be only about 5 μA. However, the actual numerical parameters of the diodes used are not available to allow comparison with analytical results.

Our analysis involves several approximations, and the result is accurate only for moderate rf voltage swings and photocurrents. Also, the effect of circuit tuning is completely neglected. We believe that in a real oscillator the interaction of the device and the circuit can

play a major role in determining the injection locking efficiency. A more rigorous analytical approach is being taken to obtain results that are applicable under even large-signal operations.

It is interesting that injection locking with an input signal proportional to sin 2/3 ωt is also possible. $J_{2/3}$ can generate $E_b \propto \sin 2/3\ \omega t$, and, from Eq. 27, $e^{-x\cos\omega t}\ e^{y\cos 2/3\omega t}$ contains a term $(I_1(x) \cos \omega t)\ (I_3(y) \cos 2\omega t)$ that produces a current component at $\cos \omega t$. This current component then acts as the driving injection signal. Similarly, any multiples of the subharmonics are possible injection locking signals as well.

In conclusion, we have shown that subharmonic optical injection locking of Si IMPATT oscillators can have a locking range of $\sim$100 MHz if modulated optical signal can be efficiently converted into rf photocurrent. In view of the experimental results obtained so far (more than 5 MHz of locking range with less than 5 μA of rf optical current), we feel that the calculated results underestimate the locking range, although the experimental device parameters are not known well enough to allow careful comparison. Nevertheless, we do not see any fundamental reason why this scheme will not work at millimeter-wave frequencies.

SECTION 3

RECENT RESULTS ON OPTICAL INJECTION LOCKING OF Si IMPATT OSCILLATORS

Last quarter we reported some initial results on the successful optical injection locking of X-band Si IMPATT oscillators. We achieved locking of an 8.754-GHz IMPATT oscillator by injecting an optical signal modulated at 2.918 GHz. We also observed a reduction of oscillator side-band noise through optical-illumination and injection-locking processes. In this quarter, we continued the experiment with particular emphasis on obtaining the locking range versus locking gain relation for various orders of subharmonic injection signal.

The injection-locking characteristics of IMPATT oscillators were found to depend heavily on the cavity tuning conditions. If the cavity was tuned such that the IMPATT oscillated with a high Q factor (i.e., narrow spectral width and minimum side-band noise), the locking range typically was very small (a few hundred kilohertz). However, if the cavity was tuned for low-Q oscillation, then the locking process became very efficient. This observation agreed well with our theoretical calculations, given in Section 2. Another factor that affected the injection locking process was the dc bias of the IMPATT diode. We found that, depending on the bias condition of the diode, different amounts of IMPATT oscillation frequency shift could be observed for a fixed dc optical illumination. Under certain conditions, the frequency shift was positive; but, for different combinations of circuit tuning and dc bias, it could also be negative. In general, a large locking range was obtained if the oscillator frequency shift due to optical illumination was large.

One of our IMPATT oscillators, when biased at 28 mA and tuned to 8.116 GHz, could be optically injection locked to several different orders of subharmonics. Figure 4 shows the changes of oscillator spectrum at five different injection signal power levels. From Figure 4(a) to Figure 4(d), the injection signal level was raised from -20 dBm to 10 dBm in 10 dBm steps. As shown in Figure 4(a), the oscillator output was initially at 8.111 GHz while the injection signal was at roughly

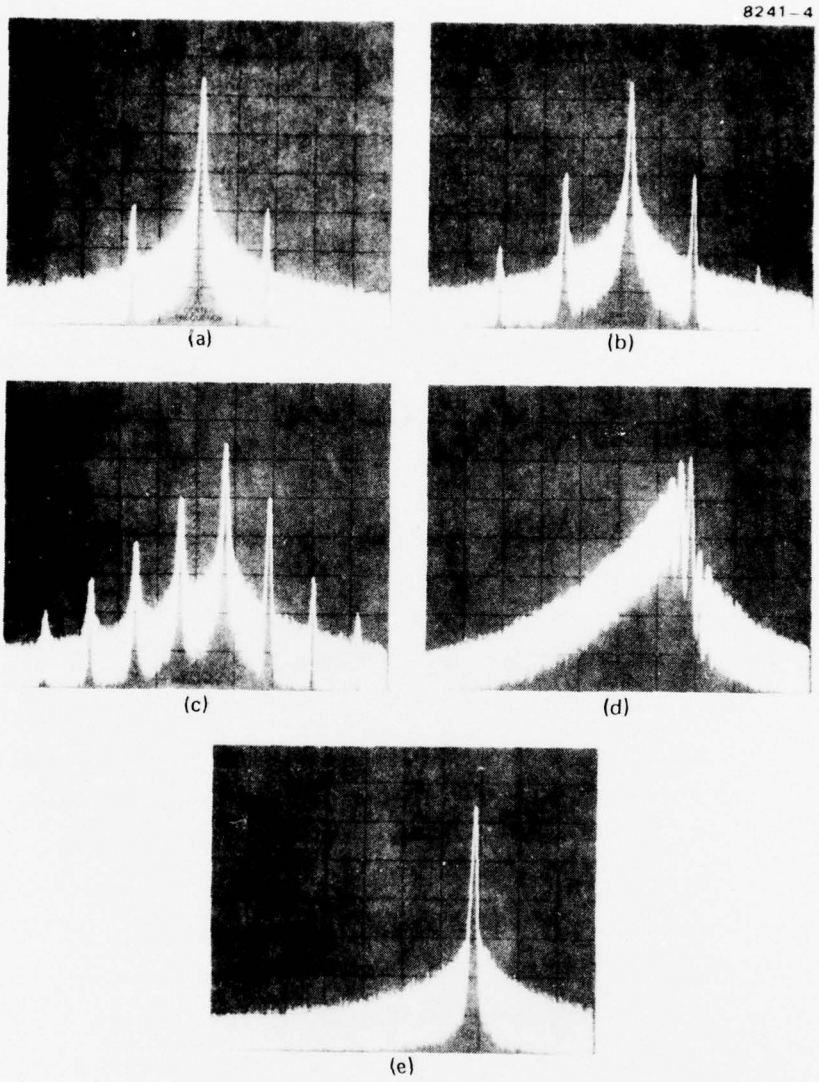

Figure 4. Spectra of an injection-locked IMPATT oscillator at various injection signal levels.
IMPATT oscillation frequency: 8.111 GHz
Injection signal frequency: 1.352 GHz
Horizontal scale: 2 MHz/div
Vertical scale: 10 dB/div
Reference level: 30 dBm.

one-sixth of 8.1146 GHz, or 1.3524 GHz. However, as shown in Figure 4(e), when injection locking finally took place, the oscillator frequency was pulled in and locked to the sixth harmonic of the injected signal frequency.

Figure 5 is a plot of the locking band versus locking gain of the same IMPATT oscillator for several different subharmonic orders. The IMPATT oscillation frequency was at 8.116 GHz. A frequency ratio as high as 8:1 was used (i.e., the injection signal was running at 1.014 GHz) to achieve injection locking. The locking gain was defined as the ratio of the IMPATT oscillator output power to the microwave power used to modulate the injection laser. Therefore, the plot of locking band versus locking gain actually contains the information on modulation response of the injection laser as well. For instance, the modulation depth of the laser at 2.03 GHz (4:1 frequency ratio) was not as efficient as at 1.35 GHz (6:1 frequency ratio); therefore, the injection locking efficiency of the 6:1 subharmonic was better than that of the 4:1 subharmonic when the locking gain was greater than 8 dB. It is also interesting that in our oscillator the even order of subharmonics is preferred to the odd order of subharmonics with respect to the injection locking efficiency. We believe that this is a result of the particular cavity tuning. Further studies are needed to clarify this point.

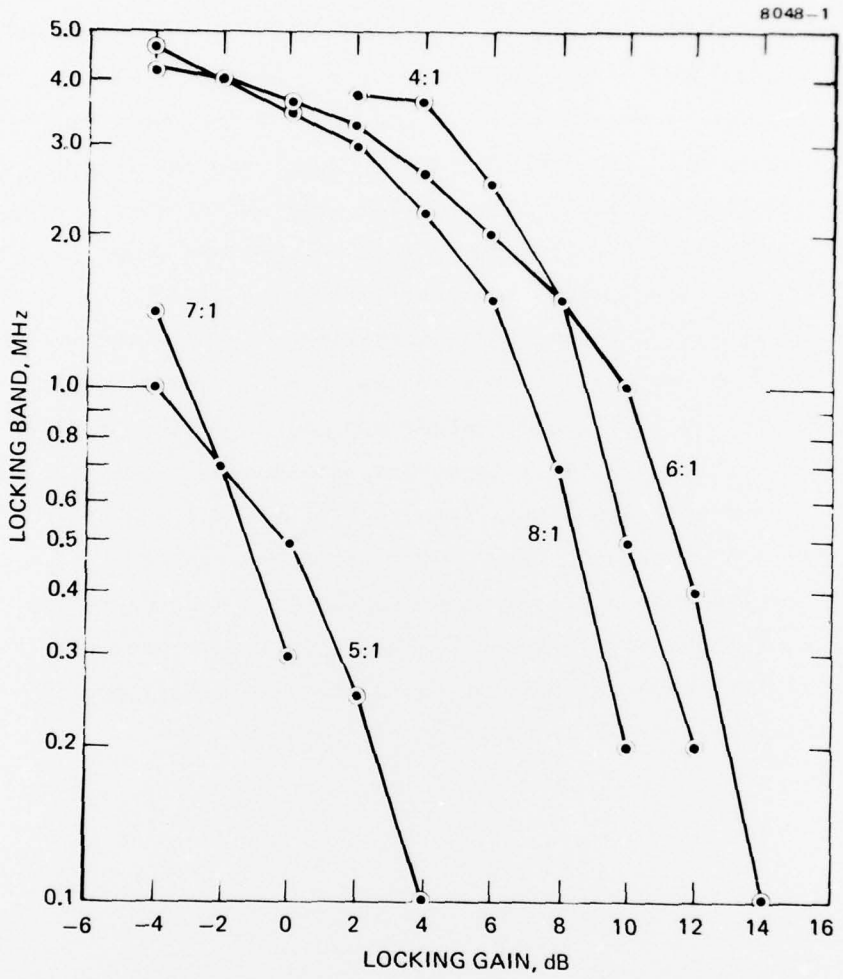

Figure 5. Locking band versus locking gain of a subharmonically optically injection-locked IMPATT oscillator.

SECTION 4

MODE LOCKING OF INJECTION LASERS

In the last report, we discussed the general effects of laser medium dispersion, laser relaxation oscillation, and the laser spectral broadening mechanism on the success of mode-locking GaAs injection lasers. The first demonstration of injection laser mode locking at MIT[4] was achieved by using an external-cavity configuration and by varying the current through the laser diode at a rate determined by the photon round-trip transit time in the cavity. This section expands on that discussion with emphasis on the effects of different external cavity configurations.

One of the reasons for using an external cavity for injection laser mode locking is to reduce the required gain modulation frequency to a few gigahertz. Without an external cavity, the required frequency f is 80 to 130 GHz for typical diode lengths (300 to 500 μm), where

$$f = \frac{c}{2n\ell} \quad ,$$

c is the speed of light, n is the index of refraction of GaAs, and ℓ is the diode length. Since the modulation response of the laser decreases sharply beyond a few gigahertz, it would be extremely difficult in the 80- to 130-GHz range. Theoretically, it is possible to achieve laser mode-locking with infinitesimal perturbation if the driving frequency is exactly equal to the transit time frequency.[5] Practically, however, there are several limitations. First, there will always be some detuning caused by mechanical vibrations and temperature fluctuations. Second, the phase noise in the signal source and in the laser output will also effectively detune the driving frequency. Thus, there is a minimum perturbation needed for mode locking. This sets a maximum frequency usable for mode locking an injection laser. By using an external cavity, the problems associated with very high frequency laser modulation can be circumvented.

Another reason for using the external cavity configuration is that the effects of material dispersion can be reduced significantly. This is because of the large dispersion-free air space in the optical cavity, which renders the gain medium dispersion insignificant since it constitutes only about 1% of the total cavity length. The material dispersion effect is important in an injection laser without external cavity since, in that case, the longitudinal modes of the laser are spaced unequally. However, under mode-locked conditions, the mode spacings of the locked longitudinal modes are equal. That means that the gain perturbation should be strong enough to pull the modes to their proper frequency locations in order to lock them together. Again, this will set a limit on the minimum input driving power required to obtain a given mode-locked laser pulsewidth (which is inversely proportional to the number of modes locked) or on the minimum pulsewidth obtainable for a given input driving power.

To induce coupling between longitudinal modes of a laser requires a gain (or loss) modulation with spatial dependence. The coupling coefficient between two longitudinal modes can be expressed as[5]

$$\kappa_{a,b} = \iiint_v \Delta g(x,y,z)\ E_a(x,y,z)\ E_b(x,y,z)\ dxdydz\ ,$$

where E_a and E_b are two normal modes of the laser cavity, Δg is the gain variation, and the integral is over the cavity volume v. Since E_a and E_b are orthogonal, i.e.,

$$\iiint_v E_a \cdot E_b\ dxdydz = 0\ ,$$

Δg should be a nonuniform perturbation if the coefficient of mode coupling is to be nonzero. The use of an external cavity provides a convenient solution for this problem.

There are two external-cavity configurations that can be used for the injection laser mode-locking experiment. We will examine their transmission characteristics and determine which configuration is more suitable for our purpose. The two configurations are shown in Figure 6. In Figure 6(a), the cavity is formed by one cleaved facet (A) of the semiconductor laser and an external mirror with high reflectivity ($r_3 = 0.98$). An AR coating is applied to the other facet (B) of the semiconductor laser. Figure 6(b) shows a more complicated external cavity, which is essentially the same as the first cavity except that there is no AR coating on facet B. The transmission characteristics of these resonators can be analyzed by regarding the composite resonators as one simple Fabry-Perot resonator of length ℓ_o. One of the mirrors of this equivalent resonator is mirror C, the other is the semiconductor laser. The semiconductor laser itself is a Fabry-Perot of length ℓ_1; its equivalent transmission and reflection coefficient can be calculated easily. Thus, the composite resonator transmission coefficient is

$$T = \frac{T_1 T_2 T_3}{[1-r_1 r_2 \cos\delta_1 - r_2 r_3 \cos\delta_o + r_1 r_3 \cos(\delta_o+\delta_1)]^2 + [r_1 r_2 \sin\delta_1 + r_2 r_3 \sin\delta_o - r_1 r_3 \sin(\delta_o+\delta_1)]^2} , \quad (30)$$

where

$$T_1 = t_1^2$$

$$T_2 = (t_2')^2$$

$$T_3 = t_3^2$$

$$\delta_1 = \frac{4\pi n \ell_1}{\lambda_o}$$

$$\delta_o = \frac{4\pi \ell_o}{\lambda_o}$$

n = index of refraction of GaAs

λ_o = laser wavelength in vacuum.

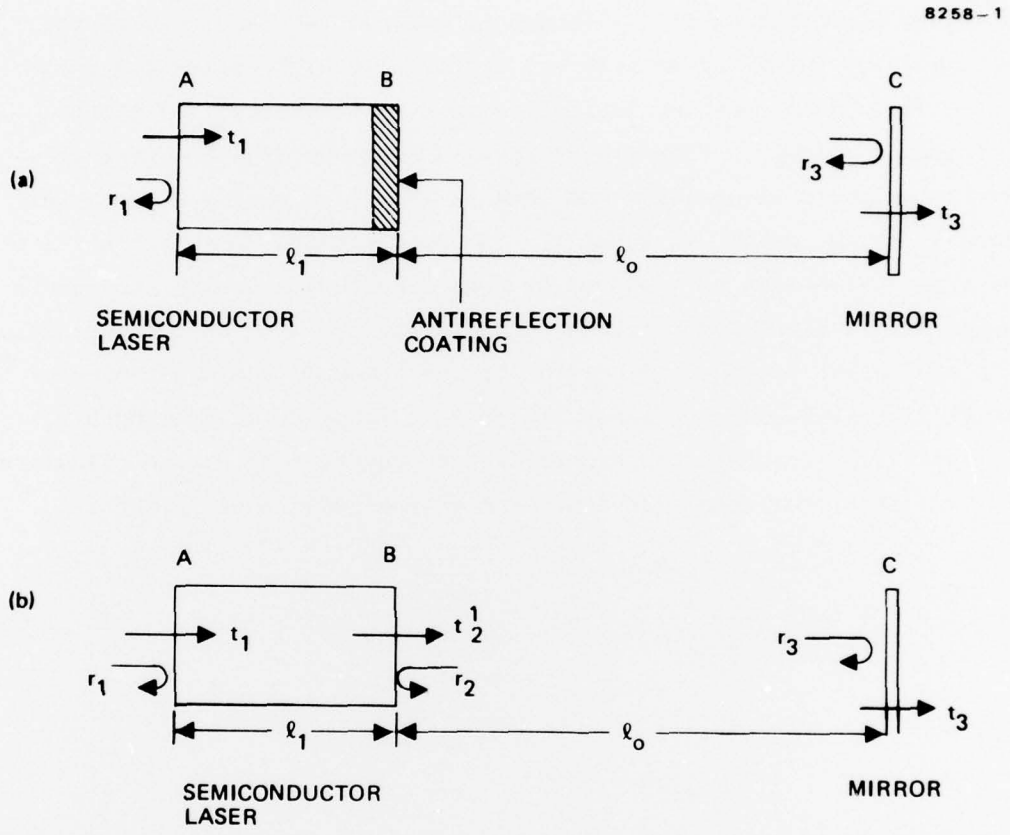

Figure 6. Two different external-cavity arrangements for semiconductor lasers.

Eq. 30 gives the transmission characteristics of the cavity shown in Figure 6(b). If we use parameters typical of the GaAs laser and let $r_3 = 0.98$, Eq. 30 can be plotted as shown in Figure 7. It exhibits the fine longitudinal mode structure of a cavity with length $\ell_o + \ell_1 \approx \ell_o$ and the beating effect of the two cavities of length ℓ_o and $\ell_o + \ell_1$. The beat frequency is $c/2n\ell_1$. If we set $r_2 = 0$ and $T_2 = 1$ in Eq. 30, we can also plot the transmission characteristic of the cavity shown in Figure 6(a). This is displayed in Figure 7. Since the cavity structure is basically a simple Fabry-Perot, the familiar equally spaced, equal height transmission pattern is obtained, as shown in Figure 8. However, the cavity Q is much lower in the simple structure. This can be seen by comparing the height and width of the transmission peaks given in Figures 9 and 10. We believe that the three-mirror cavity is a better configuration for the mode-locking process because of the higher Q factor and the additional beating effect (which forces longitudinal modes to be locked in groups). Therefore, the locking process would be more stable in this case.

Experimental work is underway. An external cavity injection laser has been set up. We have observed laser threshold current reduction due to the addition of the external mirror. More experimental results will be presented in the next quarterly report.

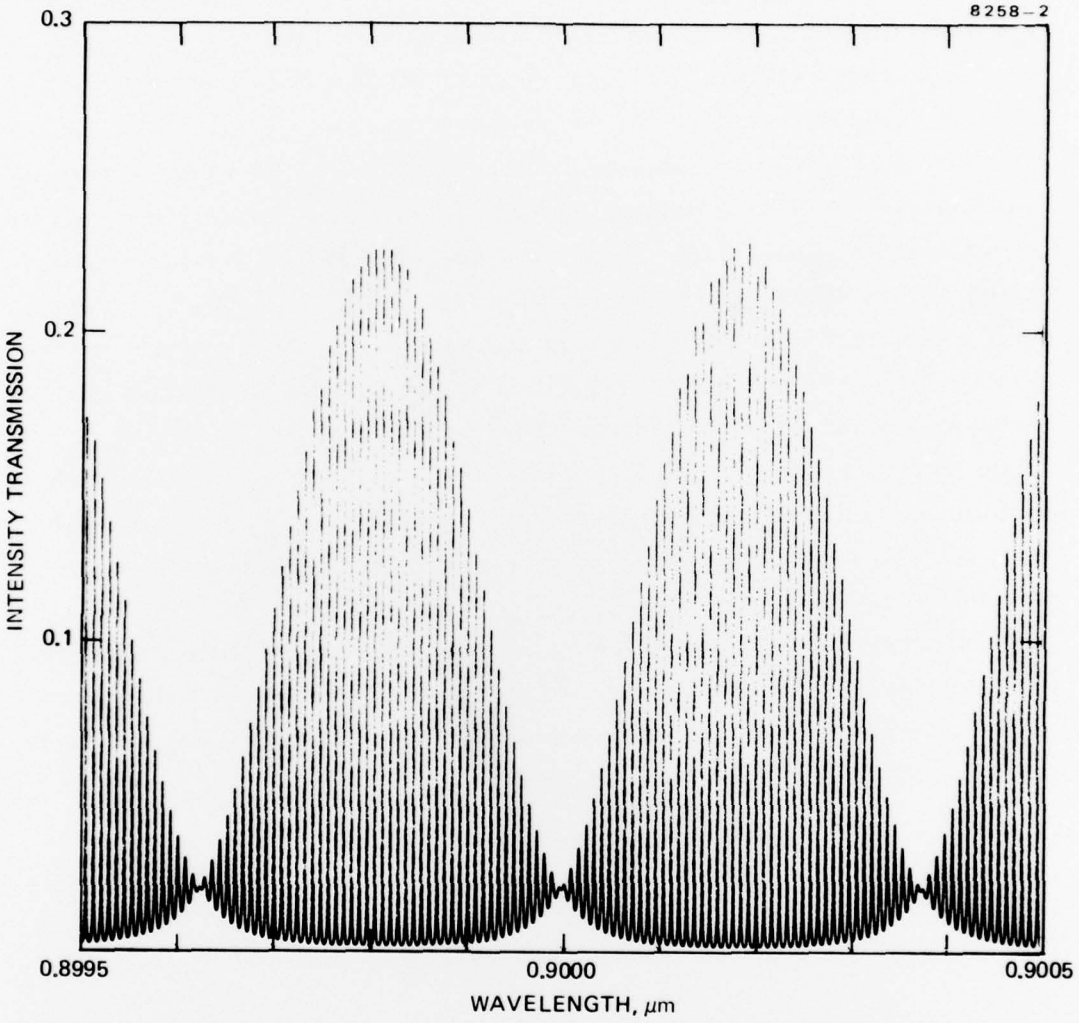

Figure 7. Intensity transmission characteristics of the three-mirror cavity depicted in Figure 6(b).

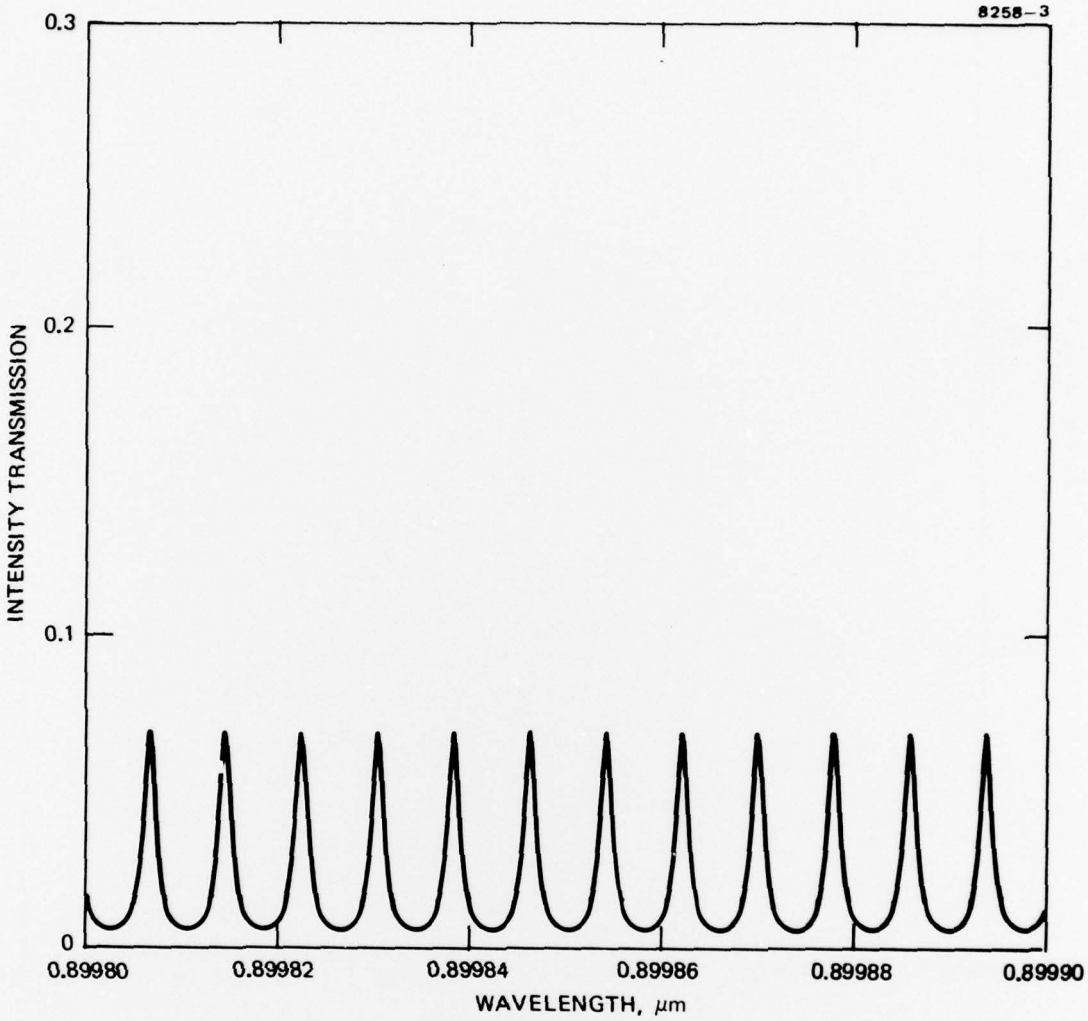

Figure 8. Intensity transmission characteristics of the simple Fabry-Perot shown in Figure 6(a).

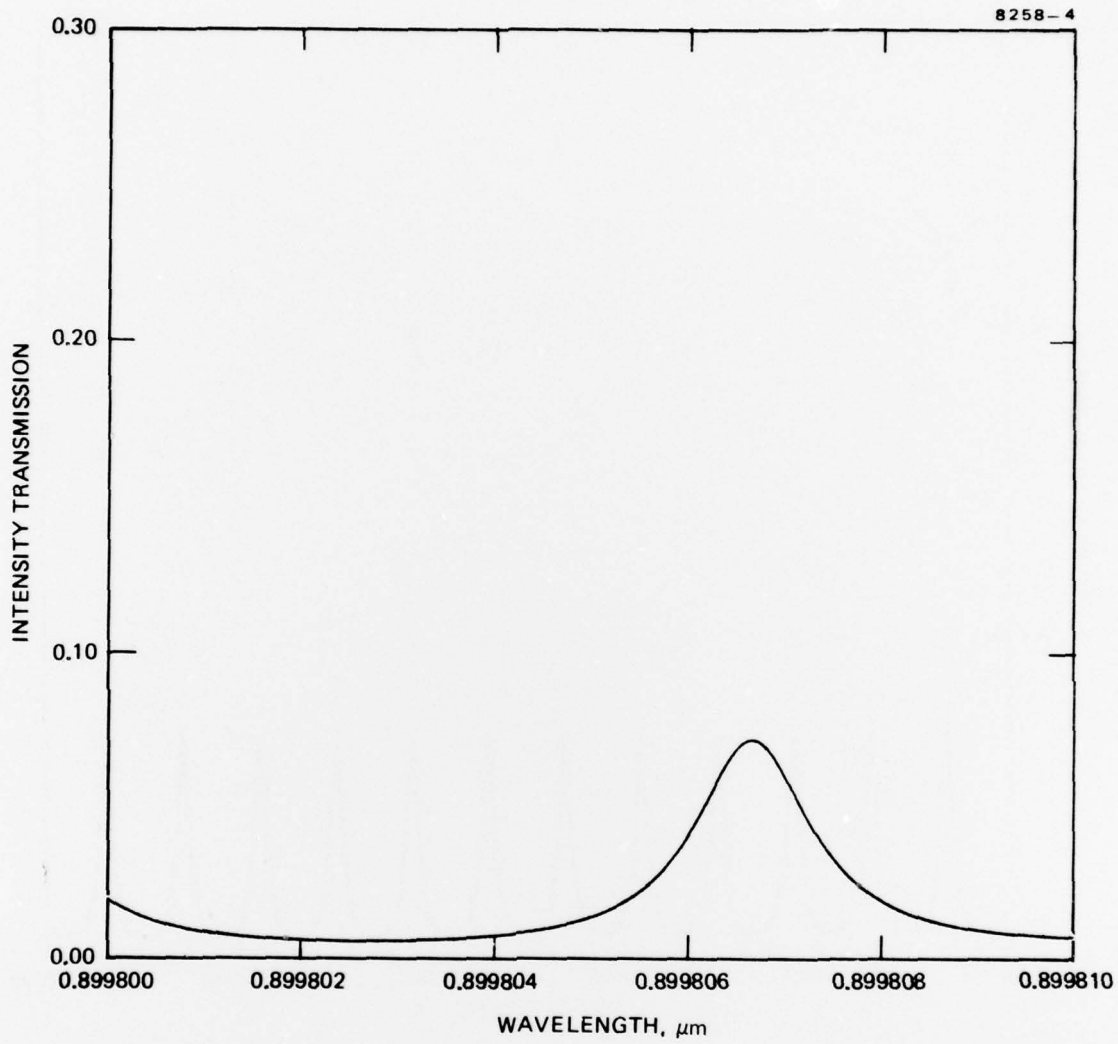

Figure 9. Resonance transmission peak of the simple cavity shown in Figure 6(a).

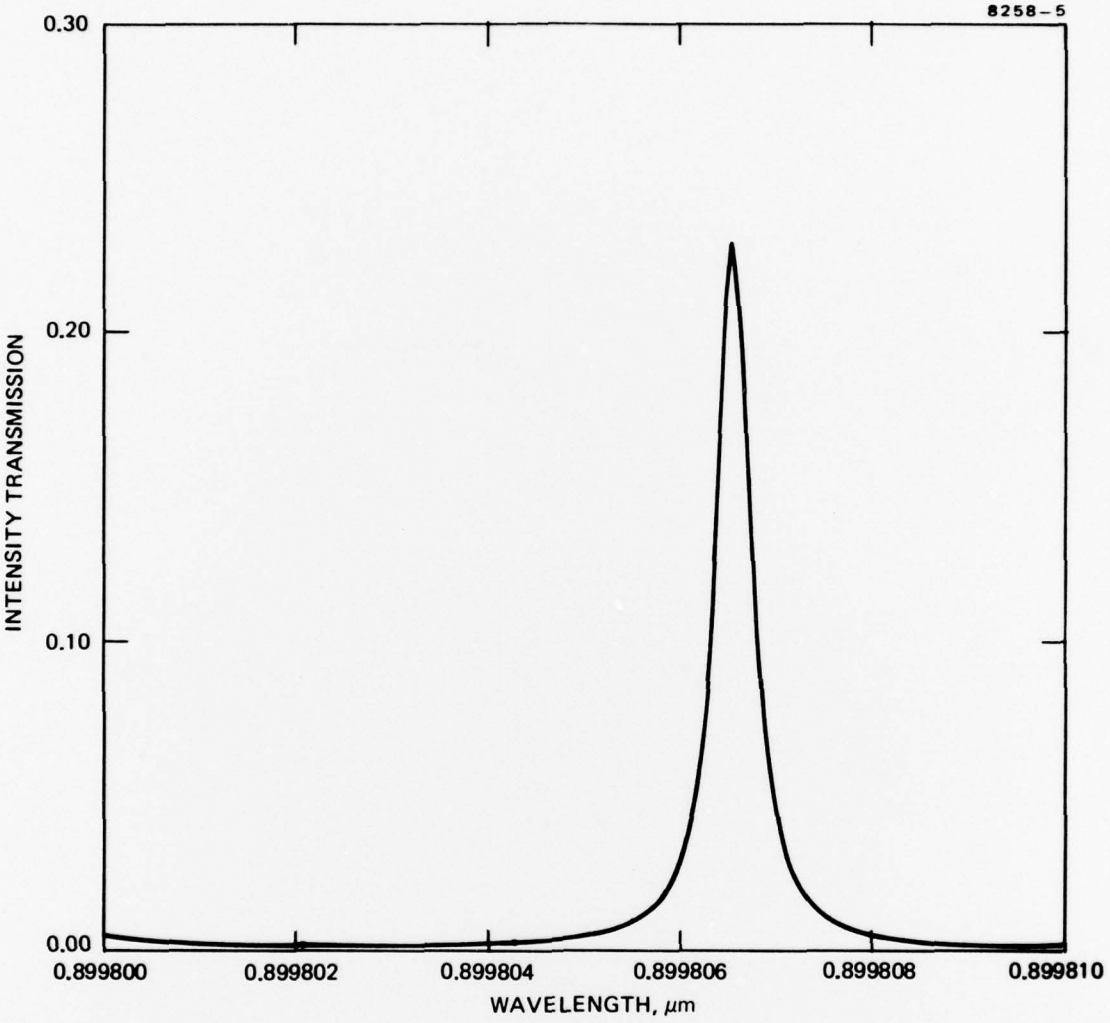

Figure 10. Resonance transmission peak of the three-mirror cavity shown in Figure 6(b).

SECTION 5

PLANS FOR THE NEXT QUARTER

In the next quarter, we will continue the injection laser mode-locking experiment. Our initial results indicate that the external cavity could lower the laser threshold, although the alignment would be very critical. We will investigate a slightly different arrangement. Instead of using a highly reflective external mirror, we will use a semi-transparent mirror such that the transmitted optical power is the output of our resonator. Since this approach will eliminate the need for specially mounted laser diodes, the experiment can be carried out with lasers that have only one emitting facet accessible. Several optical-microwave devices will be analyzed and fabricated. The fabrication of waveguide-incorporated GaAs FETs is underway. The devices will be tested for their improvement in optical response. Major efforts will be focused on the study of high-speed optical-detection techniques. Our approach is to take advantage of the speed of microwave solid-state devices and the bandwidth (and possibly the gain) derived from the oscillator and amplifier circuits.

REFERENCES

1. Read, W.T. Jr., "A Proposed High-Frequency, Negative Resistance Diode," Bell Syst. Tech. J. 37, 401 (1958).

2. Carroll, J., "Hot-Electron Microwave Generators," (Arnold, 1970).

3. Forrest, J.R. and Seeds, A.J., "Optical Injection Locking of IMPATT Oscillators," Electron. Lett. 14, 626 (1978).

4. Ho, P-.T., Glasser, L.A., Ippen, E.P., and Haus, H.A., "Picosecond Pulse Generation with a GaAlAs Laser Diode," Appl. Phys. Lett. 33, 241 (1978).

5. Yariv, A., "Internal Modulation in Multimode Laser Oscillators," J. Appl. Phys. 36, 388 (1965).